Towards a Therapy for Duchenne Muscular Dystrophy: Flow Cytometry as Tool for the Characterization of Cell Surface Charge Properties

Erika Bock

Supervisor: Dr. Judy Anderson

A thesis submitted in partial fulfillment of the Honours Thesis (05.4111/6) Course

Department of Biology

The University of Winnipeg

2005

Abstract

Duchenne muscular dystrophy (DMD) is a lethal genetic disease of childhood. Presently, there is no cure. Nitric oxide (NO) plays a role in satellite cell (SC) activation and muscle regeneration. In *mdx* mice, a genetic mouse model of DMD, SCs are hyperactive due to the absence of NO, exhausting the proliferative ability of muscle. Targeting the delivery of NO to SCs would allow SCs to remain more quiescent and respond specifically to repair needs, rather than by hyperactivity. Preliminary data suggested that flow cytometry can distinguish between different types of cells using saturation binding curves. Further development of this method would inform the design of a drug directed specifically to one tissue. This study tested the hypothesis that flow cytometry distinguishes between cells with different surface charge characteristics, by (1) determining the best method for culturing primary *mdx* cells, (2) characterizing saturation binding curves of several cell types, and (3) examining changes in binding curves of *mdx* cells cultured with L-arginine. Rapid isolation and plating of cells was of chief importance in generating healthy primary cultures. Competitive-binding assays produced distinct non-linear binding curves for each cell type examined, suggesting that many factors are involved cell surface charge characterization. Treatment with L-arginine changed the binding curve of *mdx* skeletal muscle cultures. The work has implications for pharmaceutical development of new therapies.

Acknowledgements

Thank you to my advisory committee members, Dr. Ed Byard and Dr. Donna Young, and to Dr. Ric Moodie for helpful suggestions throughout the course of this project.

I would like to thank Jason Peeler, Jeff Leiter, and GuQi Wang for their assistance, sense of humor, and advice in the lab. Thanks to Ashley Wozniak for thought-provoking conversations which contributed to sparking the initial interest in this project. Cinthya Vargas' technical expertise and clear explanations were critical to the development of the technical components of this project. Her assistance with the biotinylation procedure was greatly appreciated. Thank you to Dr. Ed Rector, who was always willing to run more experiments, and whose careful and thoughtful analysis was valued highly.

I have been incredibly fortunate to have had the opportunity to work with my supervisor, Dr. Judy Anderson. I thank her for her support and enthusiasm throughout the course of this project, which has been extremely motivating. I feel honoured to have been involved in her research. She has inspired me in many ways.

Table of Contents

Page

Abstract ii
Acknowledgments iii
Table of Contents iv
List of Tables vi
List of Figures vii
List of Appendices ix
1. Introduction 1
    1.1. Duchenne muscular dystrophy 1
    1.2 Dystrophin and the Dystrophin-Associated Protein (DAP) Complex 2
    1.3 Cell and Gene Therapies 3
    1.4 Nitric Oxide and Nitric Oxide Synthase 5
    1.5 The Role of Satellite Cells in Duchenne Muscular Dystrophy 7
    1.6 Flow Cytometry as a Method to Investigate Properties of Cell Populations 10
    1.7 Hypothesis 12
2. Materials and Methods 13
    2.1 Biotinylation of Cationized Ferritin 13
    2.2 Bead Protocol 13
        2.2.1 Non-competitive Assay 13
        2.2.2 Competitive Assay 13
        2.2.3 Avidin-FITC labeling 14
    2.3 Mouse species and care 15
    2.4 Animal Dissection and Preparation of Primary Tissue for Flow Cytometry 15
    2.5 Subculture of Cells 16
    2.6 Treatment of Cells with L-arginine 16
    2.7 Preparation of Cultured Cells for Flow Cytometric Protocol 17
    2.8 Flow Cytometric Protocol for Cells 18
    2.9 Flow Cytometry 19
3. Results 20
    3.1 Preliminary Optimization of Method 20
    3.2 Beads and Early Cell Experiments 20
        3.2.1 Beads 20
        3.2.2 Cells 21
        3.2.3 Primary Cells and Cell Lines 23
    3.3 Primary Cell Experiments 24
    3.4 Cultured Cell Experiments 28
4. Discussion 31
    4.1 Experiments using Primary Cells from Whole Animals 31
    4.2 Experiments using Cultured Cells 32
    4.3 Previous Studies and the Novelty of the Competitive Binding Assay 34
    4.4 Potential for Mathematical Investigation of Cell Character 37
    4.5 Future Applications and Research Directions 38
5. Conclusions 40
6. References 41

7. Appendices....44
7.1. Flow Cytometry Data Sheet....44
7.2 Recipes....45

List of Tables

Page

1 Chart used in preparation of bead samples for flow cytometric analysis indicating volumes of diluted bead solution, biotinylated cationized-ferritin, plain cationized-ferritin, and 1x PBS 14

2 Chart used in preparation of cell samples for flow cytometric analysis indicating volumes of cell solution, biotinylated cationized-ferritin, plain cationized-ferritin, and 1x PBS 18

3 Chart used in preparation of samples for initial experiment which compared the non-competitive and competitive assays with the C2C12 mouse cell line, indicating volumes of cell solution, biotinylated cationized-ferritin, plain cationized-ferritin, and 1x PBS 18

List of Figures

Page

1 Comparison of competitive and non-competitive assays for 4.5 μm beads 21

2 Comparison of competitive and non-competitive assays for C2C12 mouse cells 22

3 Competitive binding assay on C57 and *mdx* myoblasts, C2C12 (mouse) and L6 (rat) muscle cell lines, Chang liver cell line, primary spleen cells, and 4.5 and 2.0 μm polycarbonate beads 23

4 Competitive binding assay on primary cardiac, liver, spleen, and skeletal muscle cells from *mdx* mice (Experiment 1) 25

5 Competitive binding assay on primary cardiac, liver, spleen, and skeletal muscle cells from *mdx* mice (Experiment 2) 26

6a Histogram for liver cells incubated in 5 μl BCF, displaying three peaks for number of events against FITC log 26

6b Histogram for liver cells incubated in 20 μl BCF, displaying one peak for number of events against FITC log 26

7a Histogram for heart cells incubated in 5 μl BCF, displaying three peaks for number of events against FITC log 27

7b Histogram for heart cells incubated in 20 μl BCF, with one peak for number of events against FITC log 27

8a Histogram for muscle cells incubated in 5 μl BCF, displaying two peaks for number of events against FITC log 27

8b Histogram for muscle cells incubated in 20 μl BCF, displaying one peak for number of events against FITC log 27

9 Histogram for spleen cells incubated in 20 μl BCF, displaying two distinct peaks for number of events against FITC log 28

10a Microscope slide of untreated *mdx* skeletal muscle cells, showing limited differentiation and moderate cell density 28

10b Microscope slide of *mdx* skeletal muscle cells treated with L-arginine, showing a high degree of differentiation and high cell density 28

Page

11 Experiment 3 competitive binding assay for *mdx* skeletal muscle cells cultured in the presence or absence of L-arginine 29

12 Experiment 4 competitive binding assay for *mdx* skeletal muscle cells cultured in the presence or absence of L-arginine in two rounds of culture.....30

13 The effect of ratio of BCF:CF and total level of BCF and CF in the competitive binding assay, where 1 and 2 both have 1:1 BCF:CF but at different total levels of ferritin, and 3 has 100% BCF.....36

List of Appendices

Page

7.1 Flow Cytometry Data Sheet 44

7.1.1 Example of Histogram produced for *mdx* mouse spleen cells incubated with 20 µl BCF 44

7.1.2 Statistical Printout from Flow Cytometric Analysis 45

7.2 Recipes 45

7.2.1 Preparation of Proliferation Medium for C2C12 and L6 Cell Lines 45

7.2.2 Preparation of Proliferation Medium for Primary Cells 46

7.2.3 Preparation of Hank's Balanced Salt Solution (10X) 46

1. Introduction

1.1 Duchenne Muscular Dystrophy

Muscular dystrophies are a diverse group of genetically-determined muscular disorders characterized by progressive wasting of skeletal muscle. Muscular dystrophies have been mapped to twenty-nine loci and give rise to thirty-four different phenotypes of the disease (Dalkilic and Kunkel, 2003). Muscular dystrophies often affect cardiac and smooth muscles or other tissues in addition to skeletal muscle. The patterns of inheritance for these diseases may be either dominant or recessive and may be sex-linked or autosomal, although the disease may also arise due to a new mutation.

Duchenne muscular dystrophy (DMD), the most common form of muscular dystrophy, is caused by a mutation in the gene encoding the protein dystrophin. Studies on DMD have provided new insight into other forms of the disease. As a result, in the past decade a better understanding of the genetic and cellular basis of the various muscular dystrophies has been achieved. An appreciation for the molecular basis of the muscular dystrophies is an important step in developing therapies for these devastating diseases.

DMD, one of the most common X-linked genetic diseases, is a lethal, recessive disease caused mainly by frameshift mutations in the dystrophin gene (Kolata, 1985; Aartsma-Rus *et al.*, 2004). DMD is characterized by progressive proximal weakness beginning at a very young age. The incidence of DMD is approximately 1 in 3500 boys (Brown, 1997; Dalkilic and Kunkel, 2003). Boys with DMD are wheelchair-dependent by the time they reach their teens, and most die in their late twenties due to respiratory failure (Brown, 1997). Of these occurrences of DMD, approximately one third are due to *de novo* mutations in the dystrophin gene, while two thirds are inherited from carrier mothers (Worton *et al.*, 1988).

In 1983, the gene responsible for DMD was mapped to the middle of the short arm of the X-chromosome in a dark-staining band termed Xp21 (Worton *et al.*, 1988). This discovery was followed by a rapid succession of biochemical analyses, which yielded much information on the molecular and genetic basis of the disease. It is now understood that patients with DMD have abnormal, low, or no expression of the submembrane protein dystrophin in their muscle fibers (Brown, 1997). The dystrophin protein is 427 kDa large, and is encoded by a locus of 2.4 Mbp, discovered by Hoffman and colleagues (1987).

1.2 Dystrophin and the Dystrophin-Associated Protein (DAP) Complex

This section is based on reviews by Brown (1997) and Campbell (Durbeej and Campbell, 2002; Michele and Campbell, 2003). The role of dystrophin in muscle was elucidated from studies of the structure and orientation of the protein in the cytoskeleton. Valuable information was also obtained by studying the phenotype exhibited by DMD patients in relation to the mutation in the dystrophin gene. In normal skeletal muscle, dystrophin is found along the inner aspect of the cell membrane, and contains several folded and rod-like domains. The protein also includes a cysteine-rich region which lies directly upstream of the N terminus (Kapsa *et al.*, 2003). This cysteine-rich domain is essential for correct association with the DAP complex at the sarcolemma. Dystrophin lies parallel to the surface of the membrane, and is bound by its C and N termini to other DAPs at the intracellular membrane surface. Specifically, the N terminus has been shown to bind to the F-actin cytoskeleton and the C terminus is known to interact with transmembrane proteins of the DAP complex. These proteins include the dystroglycans, sarcoglycans, and syntrophins. Through this association with other proteins, dystrophin connects the intracellular F-actin cytoskeleton with the extracellular matrix. This connectivity is thought

to provide structural support to the cell membrane, as well as mediate cell signaling between intra- and extra-cellular components of the cell.

In patients with DMD the skeletal muscle lacks dystrophin and the cytoskeleton is rearranged as a result (Brown, 1997). Several membrane-associated proteins, including the Na^+/K^+-ATPase, are downregulated and lose their anchorage to the cytoskeleton. The absence of dystrophin is also accompanied by disorganization of calcium and sodium channels and acetylcholine receptors. Not only do the cells lack dystrophin, but expression of most other DAPs is also decreased. In dystrophic muscle, the natural cycle of regeneration and degeneration of muscle cells is shifted towards degeneration. The muscle continues to cycle through necrosis and repair until the pool of satellite cells (muscle precursor cells) is depleted at which point the muscle tissue becomes incapable of repairing itself, ultimately resulting in respiratory failure and death (Brown, 1997). This understanding of the role of dystrophin explains the lethal phenotype of the disease, and underscores the importance of researching potential therapies for its treatment.

1.3 Cell and Gene Therapies

There are currently several genetic therapies being developed as potential therapies for DMD. Because it is a recessive disorder arising from a loss-of-function mutation, many efforts have been targeted at developing gene-based replacement therapies. This approach has proven to be difficult due to the large size (14.4 kb) of the dystrophin transcript (mRNA) and the location of the protein in a complex at the sarcolemma.

In 2003, a research group from Australia proposed exon skipping as a possible therapy for DMD (Wokke, 2003). The proposed therapy would work on the principle that by skipping exons with mutations, the reading frame of the dystrophin gene may be reestablished to produce a truncated, but partially functional, protein product (Mann *et al.*,

2000; Wokke, 2003). A DMD patient could then be treated to alter his/her phenotype to that of the milder Becker muscular dystrophy (BMD) phenotype. This research is still in the preliminary stage, but has been shown to be successful in dystrophic mice (Wokke, 2003). Clinical applications, however, appear to be distant.

Studies with viral vectors have imparted some capacity for dystrophin synthesis in the muscle cells of *mdx* (**m**uscular **d**ystrophy, **X**-linked) mice treated with the vector. The mice show a complete loss of dystrophin due to a point mutation, although they present a milder phenotype of dystrophy more like BMD (Bulfield *et al.*, 1984). After virally-directed transgenic dystrophin synthesis, some muscle fibers do have dystrophin present. However, long-term maintenance of the protein expression has not been achieved in animal trials, due to immune rejection of cells that express the transgene, and due to the virulence of the vector (Acsdai *et al.,* 1996; Kapsa *et al.,* 2003). Studies with plasmid vectors have shown that both partial and full dystrophin expression can be maintained in *mdx* mice for a maximum of six months (Kapsa *et al.,* 2003). As yet, neither of these methods has been tested in human clinical trials.

Transplantation of myoblasts is another method used to introduce the dystrophin gene into dystrophic muscle. Myoblasts are muscle precursor cells that can be isolated from muscle tissue and amplified by proliferation in tissue culture. Myoblast transfer involves the injection of cultured myoblasts into dystrophic muscle. It is intended that the injected cells then divide and fuse to form new muscle fibers. Several limitations to this approach include immune rejection, limited proliferation, lack of fusion into fibers due to fibrosis in the dystrophic muscle, limited spread of injected cells, and poor cell survival rates (Huard *et al.*, 2003). Recent work by Huard and colleagues has shown that muscle-derived stem cells hold

promise as a cell therapy in that they have greater ability to divide, and therefore to deliver the dystrophin gene to diseased muscle. This approach has yet to be tested in clinical trials.

A homologue of dystrophin in skeletal muscle is the 395 kD protein, utrophin. The slightly smaller utrophin protein has actin-binding and DAP-binding affinity, and is therefore functionally similar to dystrophin. During development, utrophin is expressed ubiquitously in foetal tissues (Blake *et al.*, 1992), and is down-regulated at birth. In normal adult skeletal muscle, utrophin is localized to the neuromuscular junction region on each fiber. During muscle regeneration, utrophin expression is up-regulated, suggesting that utrophin substitution might present a mechanism for the alleviation of the dystrophic phenotype in humans (Jasmin *et al.*, 2002). In *mdx* mice, further utrophin overexpression produced by transgenic breeding relieves or prevents muscular dystrophy (Rafael *et al.*, 1998). Further studies are needed to determine if this "substitution" treatment for dystrophy in mice is effective in the DMD patient.

1.4 Nitric Oxide and Nitric Oxide Synthase

Nitric oxide (NO) is a small, hydrophobic molecule produced within several tissues. The short half-life and high diffusion rate of NO make it an ideal cellular signaling molecule. As NO has a half-life of 3 to 4 seconds, its effects are limited to locations close to its site of production (Kaminski and Andrade, 2001). NO plays many roles in the body, including modulating vascular tone, acting as a neurotransmitter, and aiding in the immune response. Specific to skeletal muscle, NO is known to modulate Ca^{2+} release, modulate or partly inhibit muscle contraction, and contribute to longitudinal muscle growth by sarcomere addition (Tidball *et al.*, 1999; Reid, 2001; Stammler and Meissner, 2001). Due to its ability to form reactive oxygen species, NO is also capable of causing tissue necrosis. In high amounts, NO is toxic to tissue.

Synthesis of NO within tissues is mediated by a family of enzymes termed nitric oxide synthases (NOS) which generate NO from L-arginine, in the presence of nicotinamide adenine dinucleotide phosphate (NADPH) and oxygen. The synthesis of NO by NOS is dependent on five cofactors (Kaminski and Andrade, 2001).

Within the NOS family, there are three major isoforms of NOS: endothelial NOS (eNOS), inducible NOS (iNOS), and neuronal NOS (nNOS). All three isoforms are found in skeletal muscle, although nNOS predominates. A unique isoform of nNOS, nNOS-μ, is found in cardiac and skeletal muscle (Silvagno *et al.*, 1996). In the DAP complex, the dystrophin-associated protein α_1-syntrophin binds nNOS-μ and dystrophin, linking nNOS-μ to the dystrophin-associated complex and localizing nNOS-μ at the sarcolemma (Brenman *et al.*, 1995). The activity of nNOS is related to the intracellular levels of calcium, and also depends on calmodulin (Kaminski and Andrade, 2001).

In Duchenne muscular dystrophy and its genetic homologue, the *mdx* mouse, nNOS is absent from the sarcolemma. It is displaced to the cytosol, and both its level of activity and expression are reduced. Initially, this suggested that changes in NO production may play a role in the degeneration of muscle fibers in dystrophy (Brenman *et al.*, 1995). It was initially hypothesized by Chao and colleagues in 1998 that alterations in the location of nNOS as a result of dystrophin deficiency resulted in free radical damage to the sarcolemma by NO released in the cytoplasm. Free radical damage to the sarcolemma that would result in a weaker cell that was less able to withstand mechanical stress was proposed as the major cause of the dystrophic condition. However, the complete removal of NO production in nNOS-knockout *mdx* double mutant mice did not improve dystrophy, refuting this hypothesis (Chao *et al.*, 1998). In fact, overexpression of nNOS significantly reduced *mdx* dystrophy (Wehling *et al.*, 2001).

Additional studies further expanded this observation. The protein α_1- syntrophin is expressed predominantly in skeletal and cardiac muscle (Adams *et al.*, 1995). In α_1-syntrophin knockout mice, the expression of nNOS at the sarcolemma is absent (Kameya *et al.*, 1999). However, despite the reduction in nNOS localized at the sarcolemma and the increase in cytosolic nNOS in α_1-syntrophin knockout mice, these mice showed no major muscle fiber degeneration. This suggested that the degeneration of muscle seen in DMD is not caused solely by changes in nNOS distribution (Kameya *et al.*, 1999).

1.5 The Role of Satellite Cells in Duchenne Muscular Dystrophy

Further studies by Anderson and colleagues focusing on the activation of satellite cells provided new insights into the molecular basis of dystrophy. Satellite cells are normally located between the sarcolemma of the muscle fiber and the external lamina. Following activation, satellite cells migrate away from fibers and divide as myoblasts that then start the repair process by fusing into new muscle fibers (Anderson, 2000).

After an injury to skeletal muscle, hepatocyte growth factor (HGF) moves from the fiber to the satellite cell (Tatsumi *et al.*, 1998). In intact or undamaged muscle, HGF is sequestered in the extracellular matrix (ECM) surrounding the muscle fiber. HGF release from the ECM is initiated by NO that is released from nNOS-μ upon injury. The earliest physical indication of satellite cell transformation following activation is the co-localization on satellite cells of HGF with its receptor, c-met, and a change in satellite cell morphology (Anderson, 2000).

C-met is a tyrosine kinase receptor found at the membrane of quiescent and activated satellite cells in muscle. The binding of HGF to c-met initiates proliferation of satellite cells (Allen *et al.*, 1995). It is not yet known whether NO is capable of activating satellite cells independently of HGF/c-met signaling. This is the subject of ongoing work in

Dr. Anderson's lab (Wozniak *et al.*, 2003; Anderson and Wozniak, 2004; Wozniak *et al.*, 2005). However, studies *in vivo* have shown that NOS inhibition prevents the co-localization of HGF and c-met and prevents the enlargement of satellite cells. This suggests that the normal activation of satellite cells *in vivo* is dependent on NO.

Satellite cells are perfectly positioned to quickly respond to muscle fiber damage. NO synthesis by NOS and its release are regulated by mechanical forces. Upon shearing action during muscle damage, the NOS that is located at the sarcolemma produces NO. NO then diffuses quickly across the cleft between the muscle fiber and the satellite cell (Anderson, 2000). These observations, coupled with the observation that satellite cell activation occurs immediately upon muscle fiber damage, have led to the suggestion that satellite cell activation is directly mediated by NO release (Anderson, 2000).

Inhibition of nNOS by Nω-nitro-L-arginine methyl ester (L-NAME) prevents the immediate activation of satellite cells in normal muscle within 10 minutes following injury (Anderson, 2000). In addition, direct and indirect genetic loss of nNOS (in nNOS-knockout mice and *mdx* mice, respectively) also prevents immediate activation of satellite cells in response to injury (Anderson, 2000). The treatment of normal mice with pharmacologic agents such as L-NAME also increases the time required for HGF to interact with the c-met receptor (Anderson, 2000). In dystrophy, the absence of dystrophin results in the down-regulation of nNOS-μ gene expression. As a result, the time required for initial satellite cell activation is similar to that seen in nNOS-μ inhibited muscle and NOS knockout mice (Anderson, 2000).

In normal muscle, pulsatile release of small doses of NO from the underlying muscle fiber maintains satellite cell quiescence. By comparison, in *mdx* muscle, NOS is displaced to the cytoplasm. NO production from NOS in *mdx* muscle is therefore a diffuse, rather than

concentrated, source of NO. As a result, both the speed with which NO reaches satellite cells and concentration of NO reaching satellite cells is decreased. In humans, the larger size of the muscle fiber in comparison with *mdx* muscle fibers may further decrease the NO gradient, resulting in a more severe dystrophic condition in boys with DMD compared with *mdx* mice.

Both abnormally large doses of NO release or the absence of pulsatile NO release activate satellite cells from quiescence (Wozniak and Anderson, unpublished data). In *mdx* mice lacking dystrophin, DAPs, and nNOS, the satellite cells do not receive regular pulses of nitric oxide, and thus are activated by the absence of nitric oxide. Similar conditions are thought to exist in DMD muscle. During disease progression, the dystrophic satellite cells are initially able to proliferate and repair the diseased muscle. After a period of time, however, the ability of the satellite cells to divide is exhausted and they become senescent. Therefore, while satellite cell hyperactivity is beneficial early in the disease by promoting proliferation and muscle regeneration, ultimately, it truncates and restricts the long-term capacity for regeneration and advances the progression of dystrophy.

Recent work investigating the activation of satellite cells on single fibers from quiescence has further developed and supported the importance of NO in satellite cell activation. Activation of satellite cells on single fibers isolated from the flexor digitorum brevis muscle of mice is dependent on the level of NOS substrate L-arginine (and therefore dependent on levels of NO) and HGF levels in the medium (Wozniak *et al.*, 2003). If it were possible to administer nitric oxide to dystrophic muscle, satellite cells could better remain quiescent and respond specifically to repair needs rather than by hyperactivity. In order to be an effective therapy, nitric oxide must be directed to the damaged dystrophic muscle, and even better to satellite cells themselves, thereby minimizing side effects on other tissue in the

patient. This is a difficult task, because of the many roles nitric oxide plays in several other tissues in the body.

1.6 Flow Cytometry as a Method to Investigate Properties of Cell Populations

Flow cytometry is a powerful analytic tool in cell biology. In flow cytometry, sample particles are suspended in a suitable fluid and then passed through the beam of a focused laser. The rate at which the sample flows through the aperture is uniform, and thus light scattering is related directly to the passage of a sample particle through the beam (Lawry, 1998). Several thousand sample particles can be counted one at a time, within a very short time, and their individual parameters measured. The parameters range from size to fluorescence intensity, the latter in the case of fluorescently-labeled particles. A data set representing the measured parameters is then collected from the sample population. The power of flow cytometry lies in the ability to sort the sample population based on these characteristics and to measure large numbers of particles within a population. Using commercial software, the data can be grouped to represent the various sub-populations within the sample (Lawry, 1998).

Routine analyses of cell surface charge are conducted using methods such as electrophoretic mobility, galvanotaxis, and isoelectric focusing (Makino *et al.*, 1993; Mycielska and Djamgoz, 2004). All of these approaches distinguish the cell surface charge based on the migration of cells in an electric field, due to their net charge, towards a positive or negative electrode. Carter and colleagues (1989) extended the notion of electrophoresis on cells to sort by charge character using flow cytometry with a fluorescent label linked to the cells via cationized ferritin molecules. Their study was also directed towards determining one data point, the net surface charge on a cell, and can be thought of as a one-dimensional assay.

Preliminary data from work in Dr. Anderson's laboratory suggested that a protocol using flow cytometry could distinguish between different types of cells even more comprehensively. This idea was extended to incorporate the use of a competitive binding assay, where cationized ferritin (CF) and biotinylated cationized ferritin (BCF) in a mixture compete for negatively charged sites on cells. Cells that are more highly charged bind more BCF and CF, both of which compete for the same individual binding sites on the surface of sample particles. After combined labeling with mixtures of different ratios of BCF and CF, the surface charge is represented by a fluorescent tag that is subsequently bound to the BCF. The cells are then fluorescently-labeled in relation to their surface charge. The competition between the larger BCF molecules and the smaller CF molecules would be expected to provide more information about the 3-dimensional characteristics of the cell surface than a non-competitive assay using only BCF. In a non-competitive assay, BCF would be free to bind any anionic site on the cell surface. The competition between BCF and CF would modify the binding of these molecules to the cell surface, and binding would then be dependent on relative charge, charge distribution, and cell size. This method would thereby rely on the ability of flow cytometry to sort a cell population with varying degrees of fluorescence intensity, which is theoretically related in some manner to the cell surface charge character.

This approach could provide more highly detailed information on the character of the cell surface than previous methods by "titrating" or exploring surface charge through the use of a competitive binding assay where BCF is in competition with CF for binding sites at the negative charges on a cell surface. The cell surface was proposed to have the potential to represent some fairly unique phenotype of the cell type. This competitive binding assay is proposed to provide a method for the characterization of cell surface charge.

1.7 Hypothesis

The hypothesis to be tested was that flow cytometry can be used to characterize and distinguish between cells of different tissues from the *mdx* mouse animal model. The hypothesis was tested in three steps. The first objective was to determine a reliable method for isolating and culturing primary cells. The second objective was to characterize the saturation binding curves of the different types of cells that were isolated. The third objective was to examine changes in saturation binding curves of cells cultured in the presence of the NOS substrate L-arginine.

If different cell types can be distinguished from one another based on cell surface charge, this property would be useful in drug development: it would enable a drug to be targeted to one specific tissue type by designing a drug molecule to bind most strongly with a cell having a particular surface charge. For example, to treat DMD, a new drug could be targeted to skeletal muscle. Similarly, if relative cell surface charges among dystrophic mouse cells are distinct from one another, the finding would allow drug developers to take advantage of the differences in cell surface charge between different tissues to deliver nitric oxide specifically to the muscle tissue. Observing changes in the binding curves of a tissue type in response to a potential drug molecule could also indicate whether exposure to that drug changes the cell surface charge properties of that tissue type, which might create an opportunity to treat cells, based on newly available or unavailable surface charge properties on that tissue type.

2. Materials and Methods

Experiments were designed to develop the BCF/CF competitive binding assay with (1) standardized negatively-charged beads and tested on (2) different cell lines, (3) cultured cells isolated from different tissues in *mdx* mice, (4) freshly isolated cells from *mdx* mice and (5) *mdx* muscle cells grown with or without L-arginine. Methods are summarized below.

2. 1 Biotinylation of Cationized Ferritin

Biotinylation of cationized ferritin (440 kDa, Sigma Chemical Co., Rochester NY) was carried out using the Immunoprobe™ Biotinylation Kit from Sigma-Aldrich (catalog # BK-101). There were 4-6 moles of biotin (244 Da) on each mole of protein (cationized ferritin), according to calculations from an assay at completion of the procedure.

2.2 Bead Protocol

2.2.1 Non-competitive Assay

Three drops of 4.5 μm *Polystyrene Microspheres* from Polysciences, Inc. (Warrington, PA) were added to 2 ml of 1x phosphate buffered saline (PBS). A 100 μl aliquot of the above solution was added to 2 ml 1x PBS. Eighty microliters of the second solution was diluted with 120 μl 1x PBS. BCF (0-120 μl, at a concentration of 1.02 mg/ml) was added to the sample, and avidin-FITC labeling and flow cytometric analysis (described in sections 2.2.3 and 2.9) were performed.

2.2.2. Competitive Assay

Three drops of either 2.0 or 4.5 μm *Polystyrene Microspheres* from Polysciences, Inc. (Warrington, PA) were added to 2 ml of 1x PBS. A 100 μl aliquot of the above solution was added to 2 ml 1x PBS. Then, 80 μl of the second solution was diluted with 120 μl 1x PBS. This bead solution was added to each of 4 tubes containing BCF (1.02 mg/ml) and CF (10 mg/ml) according to Table 1.

Table 1. Chart used in preparation of bead samples for flow cytometric analysis indicating volumes of diluted bead solution, biotinylated cationized-ferritin, plain cationized-ferritin, and 1x PBS

Sample label	Bead volume (µl)	BCF (µl)	CF (µl)	1x PBS (µl)
A	80	0	20	120
B	80	5	15	120
C	80	10	10	120
D	80	20	0	120

The above samples were incubated for 15 minutes at room temperature. 2 ml 1x PBS was added to each tube to wash excess BCF and CF from the beads. The samples were centrifuged at 438 x*g* for 15 minutes at 4°C and then the PBS was aspirated carefully leaving the beads, BCF and CF as a pellet. A 5% milk blocking solution was prepared by re-constituting 0.1 g Carnation milk powder in 2 ml of 1x PBS. 150 µl of the milk blocking solution was added to each tube. A pipette was used to gently mix each solution. The samples were incubated for 30 minutes at room temperature. Following this incubation, 2 ml of 1x PBS was added to each tube to dilute the samples. The tubes were inverted gently to ensure complete mixing. The tubes were centrifuged at 438 x*g* for 15 minutes at 4°C. The supernatant was then aspirated slowly and carefully.

2.2.3. Avidin-FITC labelling

A 1 µg/ml solution of avidin-fluorescein isothiocyanate (FITC) was prepared by diluting 1 µl of 2.8 µg/µl avidin-FITC (Amersham Inc., Mississauga, ON) in 2.8 ml 1x PBS. Each sample was incubated in 150 µl of the avidin-FITC in the dark at room temperature for 30 minutes. The samples were then diluted for washing by adding 2 ml of 1x PBS, inverted and centrifuged at 438 x*g* for 15 minutes at 4°C. The supernatant was aspirated slowly and carefully, and the pellet was washed by being re-suspended in 2 ml fresh 1x PBS and centrifuged again under the same conditions. The supernatant was aspirated carefully,

and the pellet was re-suspended in 0.5 ml fresh 1x PBS. The samples were then transported to the flow cytometry lab for analysis.

2.3 Mouse species and care

Mice used in this study were dystrophic *mdx* mice. All animals were bred and maintained at the Central Animal Care facility at the University of Manitoba according to the regulations set by the Canadian Council on Animal Care (license #03-006/1 to Dr. Anderson).

2.4 Animal Dissection and Preparation of Primary Tissue for Flow Cytometry

Three *mdx* mice were collected and transported to the laboratory. The procedure was carried out in a fume hood. Mice were euthanized by ether and killed by cervical dislocation. The skin was removed and the liver, spleen, skeletal muscle from the lower limbs, and cardiac tissue were harvested and each tissue was placed into a different autoclaved glass Petri dish. Following careful removal of connective tissue with sterile razor blades and forceps, sterile razor blades were used to chop the tissues until homogenized.

A solution of 0.2% collagenase in PBS was used to digest tissue. Homogenates were placed into autoclaved Erlenmeyer flasks and incubated with gentle shaking for one hour at 37°C with manual swirling every 15 minutes. After digestion enzyme action was inactivated by Dulbecco's Modified Eagle's Medium (DMEM). Samples were poured through sterile Nitex gauze (80 μm pore size) into conical 50 ml centrifuge tubes. Samples were centrifuged at 438 x*g* for 15 minutes at 4°C. The supernatant was discarded and the pellets re-suspended, strained through sterile cell sieves (40 μm) to remove debris, and centrifuged again at the same settings. The supernatant was discarded and the pellets re-suspended in 10 (heart, spleen, muscle) or 40 (liver) ml 1x PBS. The different volumes were related to the volume of cells isolated from the various types of tissue. The cell suspension from each of

the four tissue types was either divided into four tubes and prepared for flow cytometric analysis (section 2.8), or plated in 15-cm culture dishes and cultured in at 37°C in an atmosphere of 5% CO_2 in DMEM.

2.5 Subculture of Cells

In culturing cells, amplification of cell number requires that a plate of cells have a period of growth, then be subcultured and divided for re-plating in more than one (usually 3-4) fresh culture plates. Cells were subcultured using the following standard trypsinization protocol. When cells reached sub-confluency (70% confluence), the media was aspirated off the dishes and cells were incubated at room temperature with 5 ml of a 1:10 trypsin-EDTA/Hank's Balanced Salt Solution mixture for 5 to 10 minutes. The dishes were checked periodically with swirling using an inverted microscope to observe when the cells had lifted from the plates. When the cells had lifted from the plates, 5 ml of warm DMEM (37°C) was added to each plate to inactivate the trypsin. The cell suspensions were pipetted into conical 50 ml centrifuge tubes and spun in a centrifuge at 438 x*g* for 15 minutes at 4°C to pellet the cells. The supernatant was discarded and the cells re-suspended in fresh warmed DMEM. Aliquots of the cell suspension were then placed in the centre of fresh 15 cm Petri dishes, and 10 ml warmed media was added. The plates were swirled to ensure uniform distribution of cells within each plate. The plates were incubated at 37°C in an atmosphere of 5% CO_2 in DMEM.

2.6 Treatment of Cells with L-arginine

Primary cells were harvested from *mdx* skeletal muscles and grown in culture under various conditions. In one experiment, muscle cells were plated on 15 cm-diameter plates coated with fibronectin and incubated in DMEM for a day. The cells were then subcultured and maintained in culture until a sufficient volume of cells was obtained (9 days). One

group of cells was treated for the last two days of culture with L-arginine (0.2 μg/ml), a substrate of NOS. The other group of cells was not treated, and served as a control group. The majority of the cells were used in preparation for flow cytometric analysis (Experiment 3). Some cells from each group were frozen in sterile Eppendorf© tubes in 1 ml aliquots at -80ºC in 5% dimethyl sulfoxide (DMSO) protectant and DMEM.

In another experiment, frozen aliquoted cells were thawed on ice, and cultured for 7 days. During the period of culture, half were exposed to L-arginine (0.2 μg/ml), refreshed every 3 days. The other half was not treated. When a sufficient volume of cells was obtained, cells were removed from the culture dishes using standard trypsinization (described in section 2.5) and washed in PBS. These cells were used in flow cytometric analysis (Experiment 4). Therefore, in Experiment 4 after two rounds of culture, there were 4 treatment groups of cells, as follows:

1. Untreated/Untreated: untreated in both rounds of culture;
2. Untreated/Treated: untreated in the first round, and treated with L-arginine in the second round of culture;
3. Treated/Untreated: treated in the first round of culture and untreated in the second
4. Treated/Treated: treated in both the first and the second round of culture.

2.7 Preparation of Cultured Cells for Flow Cytometric Protocol

When a sufficient number of cells were present, the cells were harvested from the plates as described above (section 2.5). Cell suspensions were centrifuged and the supernatant discarded. Cell pellets were re-suspended in 1x PBS. The cells were centrifuged again at 438 x*g* for 15 minutes at 4°C to wash any residual media or trypsin off the cells. Cell pellets were re-suspended in 10 ml of fresh 1x PBS. Each of the treatment groups of cells was divided into four tubes and prepared for flow cytometric analysis (section 2.8).

2.8 Flow Cytometric Protocol for Cells

Samples were prepared according to Table 2.

Table 2. Chart used in preparation of cell samples for flow cytometric analysis indicating volumes of cell solution, biotinylated cationized-ferritin, plain cationized-ferritin, and 1x PBS

Sample label	Cell solution (µl)	BCF (µl)	CF (µl)	1x PBS (µl)
A	5	0	20	120
B	5	5	15	120
C	5	10	10	120
D	5	20	0	120

The 1x PBS was added to each tube first, followed by the plain cationized-ferritin (10 mg/ml), and then the biotinylated cationized-ferritin (1.08 mg/ml). The cell solution was added last, following mixing. A pipette was used to gently triturate the solutions to ensure complete mixing. The samples were incubated for 15 minutes at room temperature. Following this incubation, 2 ml of 1x PBS was added to each tube to dilute the samples and inverted gently to ensure complete mixing. The tubes were then centrifuged at 438 x*g* for 15 minutes at 4°C. The supernatant was aspirated, and the cell pellet was incubated in a 5% milk block as described in section 2.2.2. Following rinsing with PBS and centrifugation, the supernatant was aspirated slowly and carefully to avoid disturbing the cell pellet. The avidin-FITC protocol was carried out as detailed above for bead samples (section 2.2.3).

In an experiment with C2C12 cells, Table 3 was used to prepare samples.

Table 3. Chart used in preparation of samples for initial experiment which compared the non-competitive and competitive assays with the C2C12 mouse cell line, indicating volumes of cell solution, biotinylated cationized-ferritin, plain cationized-ferritin, and 1x PBS

Sample label (x-axis)	C2C12 cells (µl)	BCF (µl)	CF (µl)	PBS (µl)
0	80	0	20	120
5	80	5	15	120
10	80	10	10	120
20	80	20	0	120
50	80	50	50	120
100	80	100	0	120

2. 9 Flow Cytometry

Flow cytometric analysis was carried out in a facility at the Faculty of Medicine, University of Manitoba. Dr. Ed Rector was contracted for flow cytometry studies. The flow cytometer was a Beckman-Coulter© Altra EPICS fluorescence-activated cell sorter (FACS). Laser power was set at 150 milliwatts. The excitation wavelength was set at 488 nm, and emission wavelength was set at 525 nm using a band-pass filter for FITC. The target population was based on either 5,000 beads or 10,000 cells, and was identified by creating a histogram of the log of side-scatter (related to particle size) against the forward-angle light scatter (FALS), related to intracellular granularity or reflectivity. Once this target population was identified, three other histograms were prepared from data collected on these gated particles (beads or cells). A histogram of FITC log (i.e. fluorescence) against FALS provided an indication of the fluorescence level of the sample. Another set of histograms was created by plotting the number of events against FITC log. These histograms allowed for the determination of the x-mean of the sample (relative mean fluorescence level). A representative set of histograms and the accompanying statistical analysis are included in the appendix.

3. Results

3.1 Preliminary Optimization of Method

Assays using polycarbonate beads (2.0 μm and 4.5 μm) were used to develop the protocol for preparing cells for flow cytometric analysis. Initial work investigated the bead concentration and determined through trial and error that approximately 500,000 bead particles were needed per sample. Bead concentrations in excess of this value appeared to aggregate. The aggregation may have increased the relative shear force experienced by the beads, resulting in large volumes of bead-dust debris. Centrifugation speed was found to be optimal at 438 x*g* for 15 minutes; under these conditions the minimal amount of bead fragmentation was observed.

Preliminary tests were performed to gain an understanding of the appropriate range of fluorescent intensity for the analysis. Beads incubated in 10% and 2% bovine serum albumin (BSA) showed similarly high levels of fluorescence. It was determined that the BSA block was not sufficient. A Carnation milk powder block (5%), in standard use in immunostaining protocols, was found to be much more effective and allowed for distinction between the blank and the sample.

3.2 Beads and Early Cell Experiments

3.2.1. Beads

Three independent experiments performed with 4.5 μm beads facilitated a comparison of non-competitive and competitive assays. The relative mean channel number (x-mean) was plotted as a function of microliters of biotinylated cationized ferritin (BCF) (Figure 1). The x-mean represents the mean fluorescence of the cell population, and was divided by the background fluorescence observed with 0 μl BCF in order to normalize the data. The x-axis for Figure 1 shows the amount of BCF in each sample; in the non-

competitive assay only BCF was added, while in the competitive assay the volume of BCF shown on the x-axis was brought up to a final volume of 20 µl with cationized ferritin (CF).

With the non-competitive assay using 4.5 µm beads, the fluorescence level rose sharply and plateaued at an amount of 5 µl BCF (Figure 1). This plateau suggests that the bead solution became saturated even at a low concentration of BCF. A competitive binding assay with 4.5 µm beads provided more detail (here, seen as more changes in slope) as the sample was not saturated as quickly (Figure 1). The plateau feature of the saturation curve was shifted to a higher level of BCF in the competitive assay. The non-linear increase in mean fluorescence level with linearly-increasing amounts of BCF suggests that factors such as interference due to size and surface contour are involved in BCF binding.

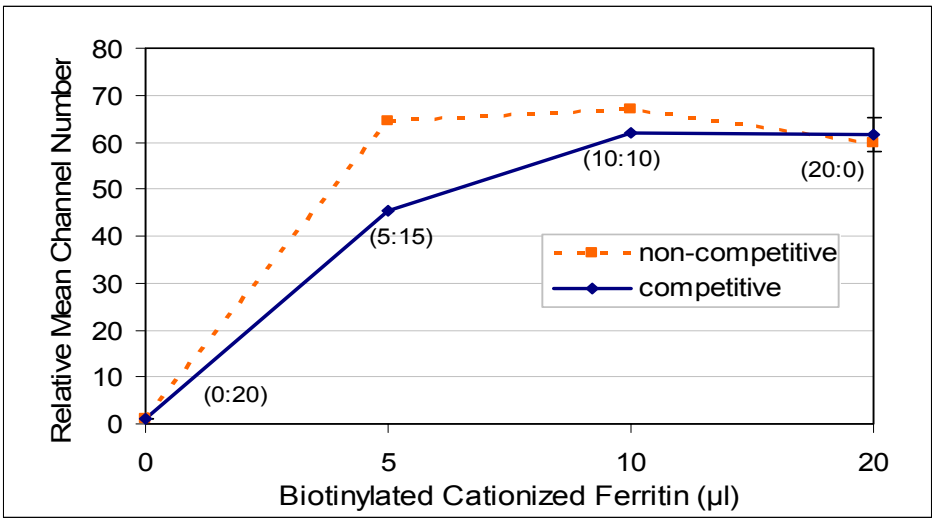

Figure 1. Comparison of competitive and non-competitive assays for 4.5 µm beads. The non-competitive assay was saturated at low amounts of BCF. The saturation point of the competitive assay (brackets show amount BCF:CF) was shifted to higher amounts of BCF.

3.2.2 Cells

The non-competitive and competitive binding assays were then performed with the C2C12 mouse cell line (Figure 2). The two curves were found to be statistically different by polynomial regression analysis ($p<0.01$, Microsoft Excel). The peak at 10 µl BCF in the competitive assay was found to be statistically different from the rest of the points on that

curve by analysis of variance. The x-axis for Figure 2 indicates the amount of BCF, not the ratio to CF in solution; ratios within the brackets represent the amount of BCF:CF for the competitive assay. The points circled in green represent solutions with 100% BCF. These samples were expected to show similar relative mean fluorescence intensity levels, as was observed. The points circled in red represent solutions with 50% BCF. At 10 µl BCF the mean fluorescence intensity is much higher than at 50 µl, indicating that a steric effect plays a role in the binding of BCF to the cell at higher total ferritin levels. Both assays showed a decrease in fluorescence at BCF amounts in excess of 10 µl.

Between 0 and 10 µl BCF, the competitive and non-competitive assays for both beads and cells were similar. The fluorescence for the non-competitive assay plateaued between 5 and 20 µl BCF, showing an early saturation feature as observed with the beads. The competitive assay provided more information, as the curve did not reach a plateau as was seen in the non-competitive assay. These results supported further development and application of the competitive assay to other cell types.

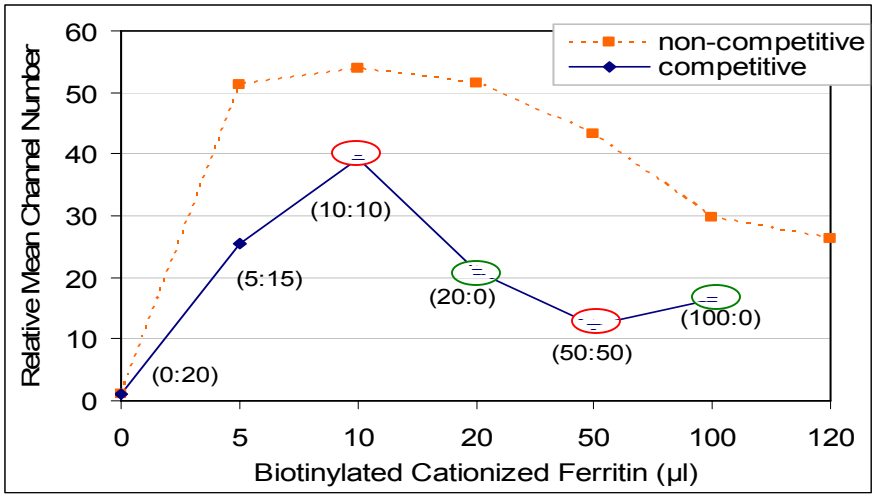

Figure 2. Comparison of competitive and non-competitive assays for C2C12 mouse cells. The non-competitive assay was saturated at low amounts of BCF while the competitive assay did not reach a plateau at a maximum level of fluorescence. Ratios within the brackets represent the amount BCF:CF for the competitive assay. Points circled in red indicate solutions with 50% BCF, while green circles indicate solutions with 100% BCF.

3.2.3 Primary Cells and Cell Lines

Next, a competitive binding assay was performed with primary muscle cells, primary spleen cells, C2C12 and L6 (rat) cell lines, the Chang liver cell line, and the two sizes (4.5 µm and 2.0 µm) of polycarbonated beads. A plot of relative mean channel number against the ratio of BCF to CF yielded saturation binding curves for each assay (Figure 3). While the curves generated for both sizes of beads were very similar, the curves for the different cell types were quite distinct from one another. While some cell types showed early saturation (*mdx* primary myoblasts, spleen primary cells, and the C2C12 mouse cell line), others (hepatocytes, the L6 cell line, and C57 primary myoblasts) did not become saturated within the experimental range of BCF:CF concentrations.

Primary muscle cells showed linear binding characteristics. These cells also had a low level of binding, suggesting that muscle cell surface charge is only slightly net negative. *mdx* and C57 primary myoblasts also showed lower mean fluorescence levels compared with the cell lines and spleen primary cells.

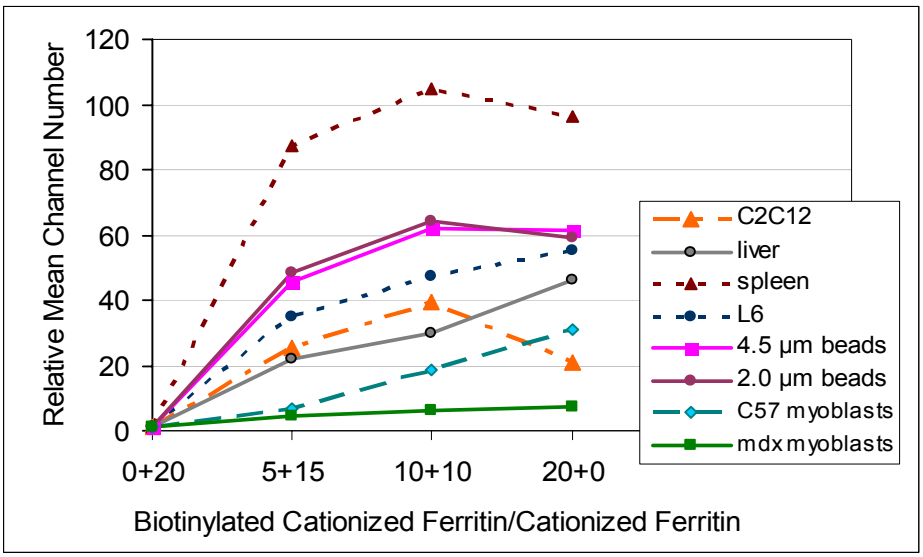

Figure 3. Competitive binding assay on C57 and *mdx* myoblasts, C2C12 (mouse) and L6 (rat) muscle cell lines, Chang liver cell line, primary spleen cells, and 4.5 and 2.0 µm polycarbonate beads. Curves generated for the two sizes of beads were very similar, while the curves generated for the different cell types were quite distinct from one another.

3.3 Primary Cell Experiments

The relative surface charge of freshly isolated primary cells from *mdx* mouse liver, cardiac, spleen, and skeletal muscle tissue was investigated using flow cytometric analysis. Two separate experiments were performed in which tissue was harvested from *mdx* animals and immediately prepared for flow cytometric analysis as described above. The large, sticky cells clogged the aperture of the Coulter Counter and therefore it was not possible to measure the cell concentration for these experiments. However, these experiments were useful in indicating that cell density in solution, in addition to cell characteristics, influences the saturation level of the BCF binding curve.

The saturation binding curve prepared for Experiment 1 (Figure 4) showed distinct binding curves for each cell type. Figure 4 indicates that BCF binding by *mdx* cardiac cells is saturated quickly. The low level of fluorescence for these cells was indicated by the low relative mean channel number at which saturation occurred. Skeletal muscle cells also showed early saturation, as well as evidence of minor steric interference at BCF amounts greater than 5 µl. Liver cells showed saturation at 10 µl BCF. The saturation of the curves for each of the tissues at higher amounts of BCF suggested that steric interference may affect binding of BCF to the cell surface when the level of BCF in solution reaches a certain point. Spleen cells, the smallest cells by comparison with large heart and liver cells and medium-sized muscle cells, were saturated at the highest relative mean channel number of the four cell types, indicating that spleen cells were more highly fluorescently labeled.

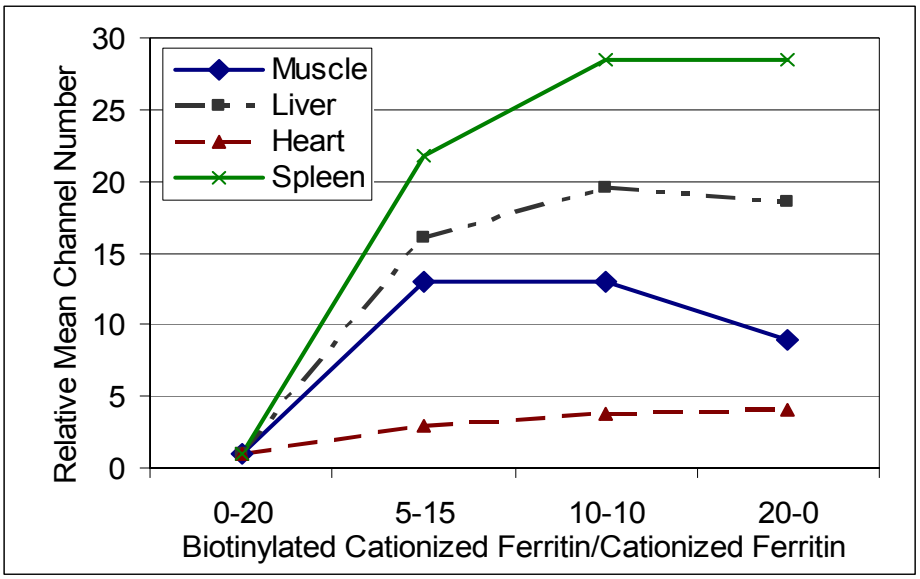

Figure 4. Competitive binding assay on primary cardiac, liver, spleen, and skeletal muscle cells from *mdx* mice (Experiment 1). Distinct binding curves were generated for each tissue type. The saturation of the curves for each of the tissues suggested that steric interference may affect binding of BCF to the cell surface at higher amounts of BCF.

A second experiment also showed distinct binding curves for each cell type. In contrast to Experiment 1, Experiment 2 showed that *mdx* liver cells were the most highly fluorescent, with spleen cells having the lowest level of fluorescence (Figure 5). Cardiac cells showed a linear curve with a low level of binding similar to that seen in Experiment 1. However, spleen, liver, and skeletal muscle cells also showed linear binding characteristics in Experiment 2, and did not reach a point of saturation. The fluorescence levels seen in the Experiment 2 were much higher than those seen in Experiment 1. Differences in cell concentrations between the two experiments likely contributed significantly in producing the differing observations for these three cell types.

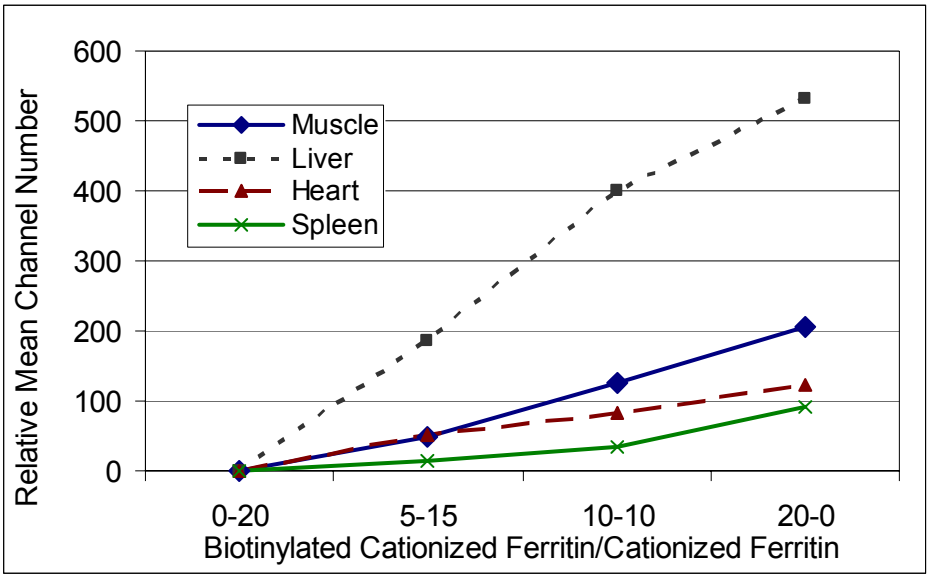

Figure 5. Competitive binding assay on primary cardiac, liver, spleen, and skeletal muscle cells from *mdx* mice (Experiment 2). Each of the curves in this experiment showed a linear increase, and the curve for each tissue type was distinct from the other tissues analyzed.

Observation of the FACS histograms displaying the number of events against FITC log for liver, muscle, spleen and heart cells showed distinct sub-populations within the initial gated population of cells. At 5 µl BCF (Figure 6a), three sub-populations within the liver cell population were clearly visible. As the amount of BCF increased, the distinction between these three groups became less obvious (Figure 6b).

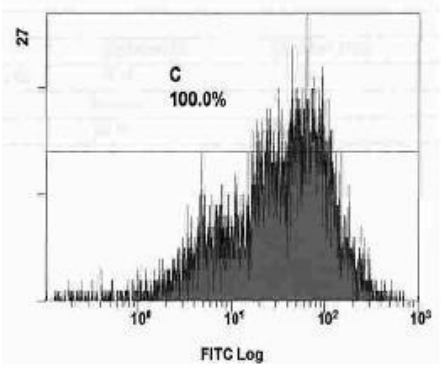

Figure 6a. Histogram for liver cells incubated in 5 µl BCF, displaying three peaks for number of events against FITC log.

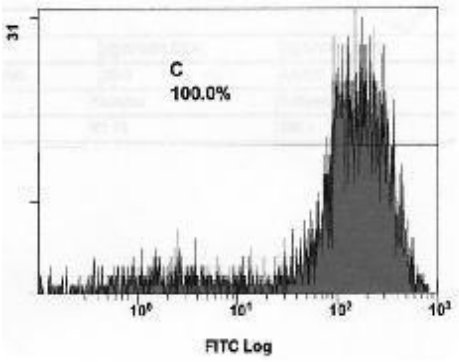

Figure 6b. Histogram for liver cells incubated in 20 µl BCF, displaying one peak for number of events against FITC log.

A similar trend was observed with muscle and heart cells. Distinct peaks, three in the heart population and two in the muscle population, were seen at 5 (Figures 7a and 8a, respectively) and 10 (data not shown) µl BCF. At 20 µl BCF, only one peak was observed for both cell types (Figures 7b and 8b).

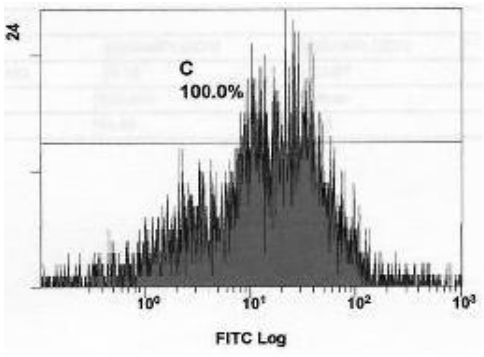

Figure 7a. Histogram for heart cells incubated in 5 µl BCF, displaying 3 peaks for number of events against FITC log.

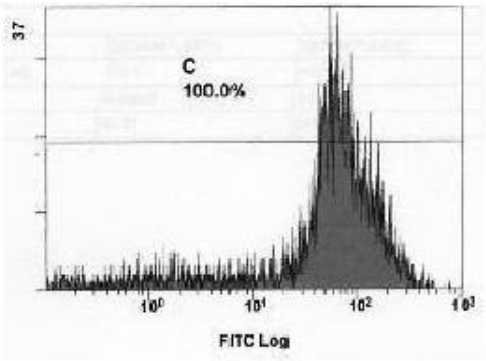

Figure 7b. Histogram for heart cells incubated in 20 µl BCF, with one peak for number of events against FITC log.

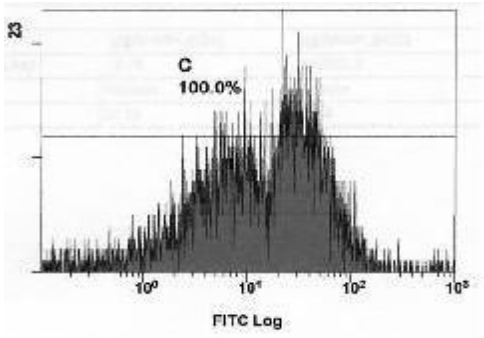

Figure 8a. Histogram for muscle cells incubated in 5 µl BCF, displaying two peaks for number of events against FITC log.

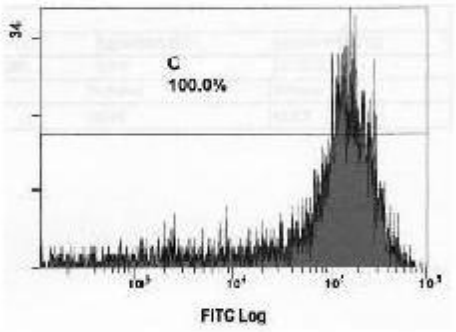

Figure 8b. Histogram for muscle cells incubated in 20 µl BCF, displaying one peak for number of events against FITC log.

Spleen cells also showed the presence of several sub-populations. This distinction was noticeable in the spleen samples even at 20 µl BCF (Figure 9).

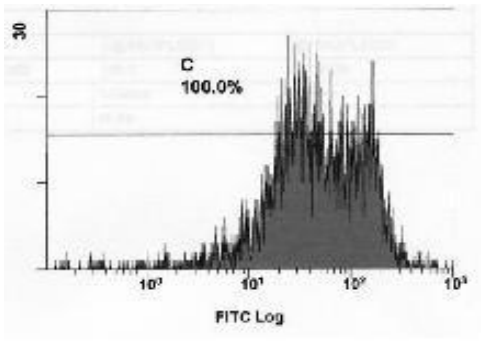

Figure 9. Histogram for spleen cells incubated in 20 µl BCF, displaying two distinct peaks for number of events against FITC log.

3.4 Cultured Cell Experiments

The change in relative surface charge of *mdx* skeletal muscle cells after culture in L-arginine was investigated using flow cytometric analysis. One experiment was performed with cells from tissue harvested from the animals used in Experiment 2. These cells were cultured for 9 days with or without L-arginine treatment, and used in Experiment 3. Observation of treatment groups showed that cells treated with L-arginine experienced faster growth and were more highly differentiated (Figure 10b) than untreated cells (Figure 10a).

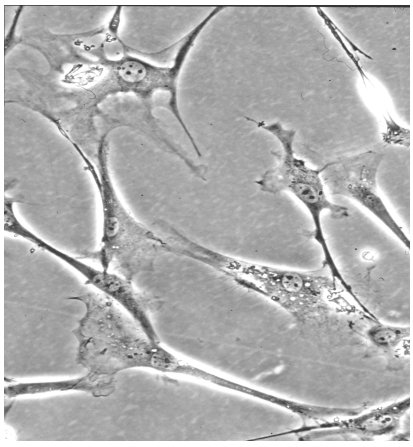

Figure 10a. Microscope slide of untreated *mdx* skeletal muscle cells, showing limited differentiation and moderate cell density.

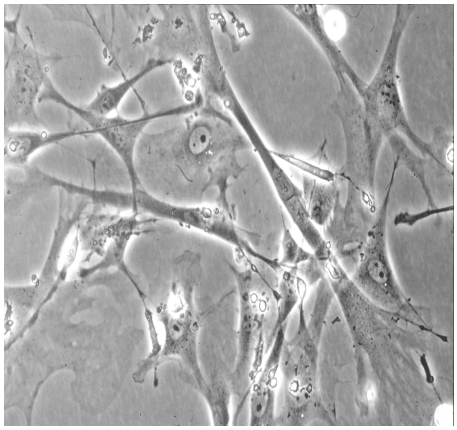

Figure 10b. Microscope slide of *mdx* skeletal muscle cells treated with L-arginine, showing a high degree of differentiation and high cell density.

A second experiment was performed using aliquots of these cells (treated and untreated) that had been frozen at -80°C in DMSO. These cells were thawed, plated, and cultured for 7 days (Experiment 4), again in the presence or absence of L-arginine.

Two sample groups were analyzed in Experiment 3: one group treated with L-arginine and one control (untreated) group. The untreated group and the treated group showed similar linear binding characteristics between 0 and 10 µl BCF (Figure 11). Between 10 and 20 µl BCF, the relative mean fluorescence level of the untreated cells rose more sharply than that of the treated cells. These results indicated that a change in the physical character of the cells, affecting BCF binding, occurred with treatment.

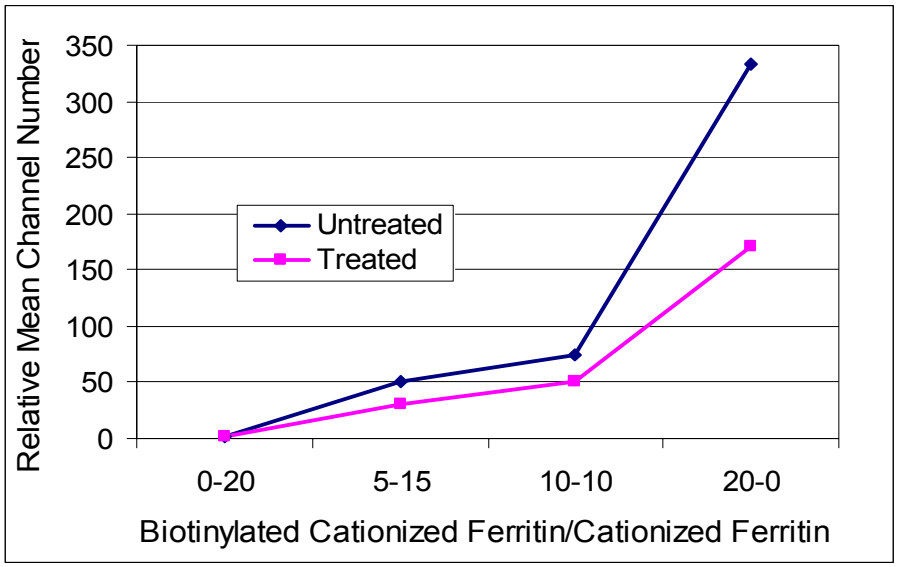

Figure 11. Experiment 3 competitive binding assay for *mdx* skeletal muscle cells cultured in the presence or absence of L-arginine. Treatment with L-arginine decreased the relative mean fluorescence level of the cells, indicating that a change in cell surface charge character occurred with treatment.

Four sample groups (as described in section 2.6 of Materials and Methods) were analyzed in Experiment 4. The two samples generated from the untreated group in Experiment 3 (untreated/untreated and untreated/treated) showed a more linear binding characteristic and had lower mean fluorescence levels than the cell samples that had been

treated in Experiment 3 (Figure 12). Cells that had been treated in Experiment 3, whether treated or untreated in Experiment 4, showed similar binding characteristics. In the same way, the curves produced for the two groups of cells not treated in Experiment 3 had similar shapes, whether or not they were treated in Experiment 4.

In Experiment 4, the cells which were treated had a higher mean fluorescence level than those cells untreated in the second round of culture. That is, the treated/treated cells had a higher mean fluorescence than the treated/untreated, and the untreated/treated had a high mean fluorescence than the untreated/untreated. This result is the opposite of that observed in Experiment 3, where treated cells had a lower mean fluorescence than the untreated cells. This result may reflect the different treatment protocols used in the two experiments, or some change in binding characteristics that is related to freeze-thaw or the DMSO protectant in which cells were frozen.

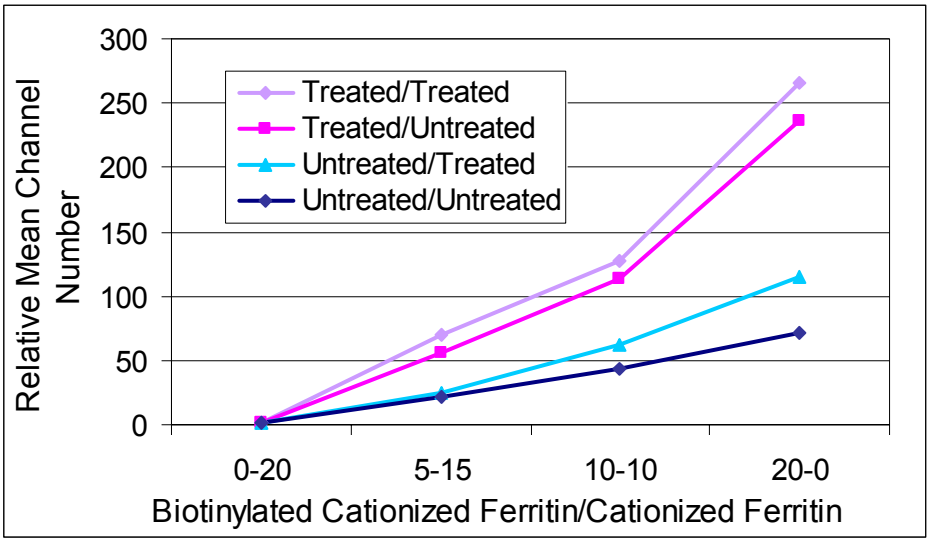

Figure 12. Experiment 4 competitive binding assay for *mdx* skeletal muscle cells cultured in the presence or absence of L-arginine in two rounds of culture. Cells untreated in the first round of culture (administered in Experiment 3) had lower mean fluorescence levels than those treated in Experiment 3. A second round of treatment (administered in Experiment 4) further increased the fluorescence levels of the cells, as seen by comparing the Treated/Untreated curve with the Treated/Treated curve.

4. Discussion

The application of flow cytometry in this project has allowed for investigation of the saturation binding curves of several particle types, including polycarbonate beads, cell lines, and primary cells. By performing competitive binding assays using biotinylated cationized ferritin and cationized ferritin, the relative mean fluorescence level at several ratios of BCF:CF was determined. Plotting the relative mean fluorescence against amount of BCF produced distinctive competitive saturation binding curves for each particle type studied. This method distinguished between primary cells from different tissues, among skeletal muscle cells from different strains that were grown in culture and subjected to different treatments, and between primary and cultured cells.

4.1 Experiments using Primary Cells from Whole Animals

Experiments performed with primary liver, spleen, cardiac, and skeletal muscle tissue isolated from *mdx* mice revealed that many factors contribute to the characteristics of the binding curve. While it was not possible to measure the cell concentration in these experiments for technical reasons, differences in cell density in the solution were observed during flow cytometric analysis since each sort is a cell count. The differences in the curves produced by the two experiments indicate that cell density in solution plays an important role in the binding characteristics of the different cell types. Each cell type produced a distinctly different binding curve from the others in both experiments. Although the trend (curve shape) was not uniformly consistent between experiments for all cell types, the curves for C2C12 and L6 cells and myoblasts were consistent across three trials in experiments with cultured cell lines. This observation indicates a potential for a high degree of sensitivity of the technique, at least for some types of cells. Further studies in which the cell

concentration was measured using a cell counter would allow for more detailed investigation into the effect of cell density in solution on the character of the binding curves.

A surface which could bind a charged fluorescent molecule without interference would be expected to show a linear curve with linearly increasing BCF concentration. However, the curves produced in these experiments were generally not linear in nature. The steric effects observed in the binding curves, resulting in a plateau or peaked curve, suggested that many factors are involved in binding of BCF to the negative charge of the particle surface. Factors such as particle size, charge distribution, and surface contour would contribute to a non-linear curve when considered in addition to charge differences between cell types. Interference due to the large size of the BCF molecules likely contributed to the non-linear nature of the binding curve. At higher concentrations of BCF, steric hindrance due to the large size of the molecules would negatively affect binding. As well, it cannot be assumed that a cell surface is necessarily uniform in the distribution of negative charges. Additional variations between the topography or three-dimensional contours of different cell types would be expected to affect BCF/CF binding competition.

4.2 Experiments using Cultured Cells

One goal of this study was to determine the best method for the isolation and culture of primary cells. The method employed in these experiments consistently resulted in the isolation of skeletal muscle cells which showed high rates of proliferation during culture. Primary cell cultures are not always as successful as the culture results from this experiment in producing highly myogenic cultures. The rapidity with which cells were isolated, washed, and plated in warm DMEM was found to be the factor of primary importance in generating healthy cultures. It is not known why the primary cultures isolated here were so enriched for myogenic cells and had so few fibroblasts.

Experiments using cultured cells provided further insight into the complexity of the binding curves. It is important to note that, while it was not possible to control the initial cell concentration, all the samples in a given curve had exactly the same concentration. Differences in concentration between experiments showed the importance of cell density in solution in the character of the binding curves: the higher concentration of cells in the second experiment shifted the saturation point to higher BCF levels, likely as there were more negatively charged cell surfaces for BCF and CF binding, reducing steric hindrance.

Treatment with L-arginine changed the binding curves from those curves generated for untreated cells, although the direction of change was not uniform between experiments. This was likely due to the vastly different treatment protocols, one with continuous L-arginine treatment and one with only the final two days of L-arginine treatment. As well, experiment 3 had cells plated on fibronectin in the initial culture. These variations were a result of different interpretations of the developing protocol by two individuals. The results from these experiments suggested that L-arginine treatment, which would increase exposure to NO during culture, somehow changes the characteristics of a cell surface. This result has important implications for pharmaceutical applications. Changes in the character of a cell surface in response to treatment could either positively or negatively impact the likelihood of a charged drug molecule binding the cell surface. Further experiments investigating the effects on the binding curves in response to drug compounds or metabolites would provide interesting information about the changes in cell surface properties due to changes in extracellular or intracellular environments. It is important to note that, while L-arginine is converted to NO by NOS inside the cells in culture, NO rapidly diffuses into the media. For this reason both internal and external cell environments could be affected by NO.

4.3 Previous Studies and the Novelty of the Competitive Binding Assay

A previous study investigated the metastatic potential of various tumour cells by examining the surface properties, including charge, of cells. The authors found that highly metastatic tumour cell lines are more likely to have a more highly negatively charged cell surface than cells with a lower metastatic potential (Carter *et al.*, 1989). The authors did not explore the applications of flow cytometry in characterizing the tumor cells, but this present study has shown that such characterization using a competitive binding assay is possible. Analysis by this method of cells from a tissue biopsy, for example, may reveal the characteristics of a tumour, conveying important information about the cell population that could then be used in developing suitable therapies. A study performed by Bauman and Bouwman (1986) investigated the use of BCF as a tool for measuring the cell surface charge of mouse bone marrow cells by flow cytometry. The authors found a good correlation between relative fluorescence intensity and cell surface charge. Their study was carried out in the interest of determining one data point, the negative cell surface charge of mouse bone marrow cells, and did not involve the use of competitive binding assays to characterize cells.

The method developed in this study provides a great degree of detail about the cell surface character by making use of existing tools and reagents in a new way, taking advantage of competition for sites on a particle surface to which a large protein molecule binds. The novelty of this method is that a competitive binding assay using BCF and CF at the level of individual cells is used to characterize a cell population. Experiments performed previously involved the binding of BCF alone, without the use of flow cytometry to measure changes in fluorescence levels due to competition with CF. Incubation with BCF alone allows for the determination of the net charge of a cell. This approach can be thought of as a one-dimensional assay. The one-dimensional approach is not capable of providing insight

into cell surface contour or distribution of charged molecules bound to the cell surface. The method developed here has the ability to convey that information because large and small molecules must compete for the same anionic binding sites, allowing for a 3-dimensional approach. Knowledge of these features of cell surfaces would be useful in developing a drug, allowing more specific targeting to a population of cells based on surface charge character.

The nature of the competitive binding assay developed here is based on observations of saturation binding curves produced in the experiments performed in this study. The competition for binding can be clarified by considering that the competition occurs at individual negative charges on the cell surface, which bind the cations on CF or BCF. Considering this, BCF and CF are competing for the same sites, whatever their number and distribution on the cell surface. Therefore, a single negative charge at a site on the cell surface will attract BCF and CF equally, and their binding is mutually exclusive at this individual site. The binding of BCF or CF to one anionic site that is in close proximity to a second anionic site will interfere with the binding of BCF or CF at the second site. If BCF binds the first site, the interference will be greater due to the larger size of BCF compared with CF. Therefore, the likelihood of CF binding the second site is greater than the likelihood of BCF binding the second site, due to the relatively smaller interference of the smaller molecule CF compared to BCF.

As well, at low total ferritin concentrations, a ferritin molecule (either BCF or CF) approaching the cell surface will be less restricted in binding an individual anionic site than at higher total ferritin concentrations, as there would be less interference between molecules approaching that site at one time. As the total level of ferritin increases there will be more molecules tying to access each individual anionic site at once. The ratio of BCF:CF also plays a role in the binding of BCF and CF to anionic sites on the cell surface. For example, if 50%

of the ferritin is biotinylated, access to the individual sites by a number of different ferritin molecules will be altered by steric interference between larger BCF molecules and smaller CF molecules. At low levels of total ferritin (and a ratio of 1:1 BCF:CF) there is an equal probability of CF and BCF binding the anionic sites on the cell surface (Figure 13.1). If the ratio is kept at 1:1 BCF:CF while the total level of ferritin is increased, the probability of BCF binding anionic sites on the cell surface is lower than that for CF, due to steric interference related to the biotin groups in the complex with BCF (Figure 13.2). That probability is also lower than for binding BCF in a lower amount of total ferritin (Figure 13.1). Essentially, the smaller CF molecules out-compete the BCF for cell surface anionic sites when the total amount of ferritin is high. At a lower amount of total ferritin there will be fewer BCF molecules to interfere with one another for binding, so the proportionate binding of BCF:CF to the cell will be closer to a 1:1 ratio. Therefore, the fluorescence intensity of a sample with 1:1 BCF:CF at a low level of total ferritin would be expected to be higher than that of a sample with the same ratio, but a higher total level of ferritin. In a solution of 100% BCF, the probability of BCF binding anionic charges on the cell surface is relatively low when compared with a 1:1 BCF:CF ratio, despite the high concentration of BCF, due to the high level of steric interference between the biotin groups in BCF as the BCF molecules approach the cell surface (Figure 13.3).

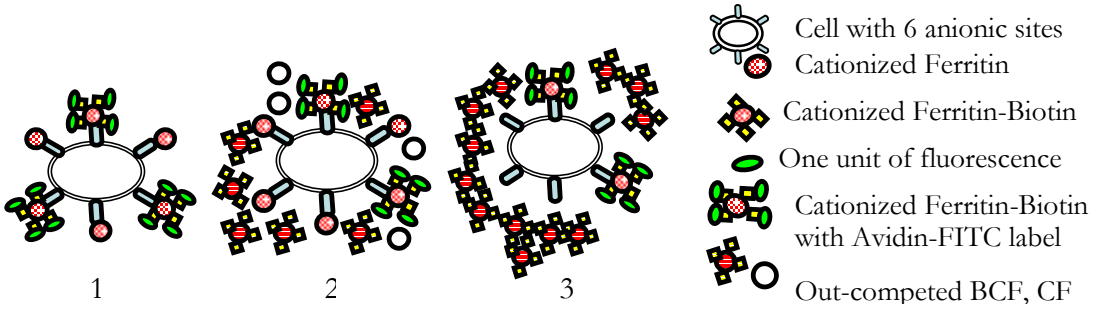

Figure 13. The effect of ratio of BCF:CF and total level of BCF and CF in the competitive binding assay, where 1 and 2 both have 1:1 BCF:CF but at different total levels of ferritin, and 3 has 100% BCF. Steric interference is lowest in 1, and higher in 2 and 3.

The distribution of charge on a cell surface cannot be assumed to be uniform, or consistent between cell types, although an even distribution is depicted in Figure 13. The competitive binding assay developed here makes use of this feature as well, as differences in charge distribution would also alter the binding of BCF and CF. For example, if one cell type was characterized by small, dense clusters of highly anionic sites around the cell perimeter, the binding of BCF and CF to this cell would be distinct from the binding to a cell characterized by widely-spaced anionic charges. The large BCF molecules would encounter more difficulty binding evenly around the former surface than the latter, resulting in another factor which would distinguish between the cell types in a competitive binding assay.

4.4 Potential for Mathematical Investigation of Cell Character

Several aspects of the surface character of cells prepared by the flow cytometric protocol could be investigated in greater detail using calculus. The integrals, intercept, and derivatives of the binding curve that describe the relative fluorescence as a function of BCF concentration can be calculated to gain a variety of information about the cell type under study. For example, integrating the mathematical function of the curve gives the area under the curve, which represents the total fluorescence, and therefore the total charge, of the sample. Calculation of the first derivative describes the slope of the curve at a particular point, representing the availability of anionic charges at the cell surface. By taking the second derivative, the inflection point representing the point at which maximum binding occurs can be determined. Thus, one advantage of this method lies in its ability to provide mathematical representations of complex interactions taking place at the molecular level. While these techniques were not undertaken in this study and would venture into complex fields of advanced organic and physical chemistry, application of these mathematical

concepts to the data would allow for quantification of data presented in the binding curves. Following this, application of statistics to the numerical data would allow further insight into the reproducibility of the method.

4.5 Future Applications and Research Directions

Application of the flow cytometric protocol using BCF to study a variety of cell types showed that numerous factors impact the character of the binding curves. These factors include cell size, surface charge, cell/bead density in solution, and likely surface contour of the particle. The degree of cell differentiation may also have an effect on the cell surface character, as shown in L-arginine experiments. The sensitivity of the method was evidenced by the ability to distinguish between sub-populations within a sample. This latter capacity to distinguish sub-populations might allow for investigation into changes in the relative proportions of particular cell features within an otherwise apparently homogenous population of cells. This would be useful in determining the different effects of disease, drug treatment, or infections on those different cell sub-populations.

This method has applications in the development of pharmaceuticals. The surface charge character determined by the competitive binding assay could be used to design drug molecules that will target unique features of a cell type, based on its cell surface character. This study was carried out in the interest of developing this method for the design of a drug-development tool with special interest in the treatment of Duchenne muscular dystrophy.

One aim of this study was to determine if the cell surface charge character of several different types of tissues would distinguish them from one another. In the case of *mdx* tissues, the skeletal muscle cell character was distinct from the other tissues. This observation suggested that the cell surface character is particular enough to allow medicinal or pharmaceutical chemists to make use of this property in the design of a new drug to

deliver nitric oxide to dystrophic muscle. For example, by designing a drug carrier molecule to carry NO which is specific to the cell surface charge character of dystrophic muscle, the specificity of NO delivery could be enhanced. The experiments presented here would need to be repeated to demonstrate replicable results under controlled, standardized experimental conditions to verify the observations. Differences between different cell types may be large enough to be detected by this sensitive method, but too small to effectively avoid non-specific drug delivery *in vivo*. Further development of this potential application would require extensive knowledge of the pharmacology of a particular drug being investigated. It also remains to be seen if cell characteristics determined *in vitro* are reflected *in vivo*, even though use of tissue culture to model *in vivo* cell populations is a standard approach. Inclusion of primary cells and cultured cells in this project attempted to investigate the potential differences between *in vitro* (modeled by cultures) and *in vivo* (modeled by primary cells) cells as much as possible in the scope of this project.

The results of this study have exciting long-term implications for industry in addition to the applications directed specifically towards a potential DMD therapy. The ability to distinguish sub-populations within a sample could be extended to distinguish between cells of different developmental or proliferative states. If developed fully, this application could be useful in numerous clinical applications.

5. Conclusions

1. Competitive binding assays provided greater insight into interactions taking place within a sample than non-competitive binding assays, as the fluorescence intensity of the samples was not saturated within the experimental amounts of BCF:CF.
2. Distinct binding curves were generated for different types of polystyrene beads, cell lines, and primary cells.
3. Treatment of *mdx* mouse skeletal muscle cells with L-arginine changed the binding curve from that observed in untreated cells in culture.
4. Cell density in solution, cell size, cell surface charge, and cell surface contour may all be involved in the generation of non-linear saturation binding curves with linearly increasing BCF concentration.
5. The BCF/CF competitive binding assay is very sensitive and shows the ability to distinguish between different populations and sub-populations.
6. The BCF/CF competitive binding assay holds potential for numerous future applications, including those originally set forth as the basis of the proposal for this study.

6. References

Aartsma-Rus, A.., Janson, A.A.M., Kaman, W.E., Bremmer-Bout, M., van Ommen, G.J.B., den Dunnen, J.T., and J.C.T. van Deutekom. 2004. Antisense-induced multiexon skipping for Duchenne muscular dystrophy makes more sense. American Journal of Human Genetics 74: 83-92.

Acsadi, G., Lochmuller, H., Jani, A., Huard, J., Massie, B., Prescott, S., Simoneau, M., Petrof, B.J., and G. Karpati. 1996. Dystrophin expression in muscles of *mdx* mice after adenovirus-mediated *in vivo* gene transfer. Human Gene Therapy 7: 129-140.

Adams, M.E., Dwyer, T.M, Dowler, L.L., White, R.A. and S.C. Froehner. 1995. Mouse alpha 1- and beta 2-syntrophin gene structure, chromosome localization, and homology with a discs large domain. Journal of Biological Chemistry 271: 2724-2730.

Allen, R.E., Sheehan, S.M., Tayler, R.G., Kendall, T.L., and G.M. Rice. 1995. Hepatocyte growth factor activates quiescent skeletal muscle satellite cells *in vitro*. Journal of Cell Physiology 165: 307-312.

Anderson, J.E. and A.C. Wozniak. 2004. Satellite cell activation on fibers: modeling events in vivo – an invited review. Canadian Journal of Physiology and Pharmacology 82: 300–310.

Anderson, J.E. 2000. A role for nitric oxide in muscle repair: nitric oxide-mediated activation of muscle satellite cells. Molecular Biology of the Cell 11:1859-1874.

Bauman, J.G.J., and E. Bouwman. 1986. The use of cationized ferritin to measure cell surface charge of mouse bone marrow cells by flow cytometry. Histochemistry 84: 454– 461.

Blake, D.J., Love, D.R., Insley, J., Morris G.E., Turley, H., Gatter, K., Dickson, G., Edwards, Y.H., and K.E. Davies. 1992. Characterization of a 4.8 kb transcript from the Duchenne Muscular Dystrophy locus expressed in Schwannoma cells. Human Molecular Genetics 1:103-109.

Brenman, J.E., Chao, D.S., Xia, H., Aldape, K., and D.S. Bredt. 1995. Nitric oxide synthase complexed with dystrophin and absent from skeletal muscle sarcolemma in Duchenne muscular dystrophy. Cell 82: 743-752.

Brown, R.H. 1997. Dystrophin-associated proteins and the muscular dystrophies. Annual Review of Medicine 48: 457-466.

Bulfield, G., Siller, W.G., Wright, P.A.L, and K.J. Moore. 1984. X chromosome–linked muscular dystrophy (*mdx*) in the mouse. Proceedings of the National Academy of Sciences (USA) 81: 1189-1192.

Carter, H.G., Partin, A.W., and D.S. Coffey. 1989. Prediction of Metastatic Potential in an Animal Model of Prostate Cancer: Flow Cytometric Quantification of Cell Surface Charge. The Journal of Urology 142: 1338 – 1341.

Chao, D.S., Silvagno, F., and D.S. Bredt. 1998. Muscular dystrophy in *mdx* mice despite lack of neuronal nitric oxide synthase. Journal of Neurochemistry. 71:784-789.

Dalkilic, I., and L.M. Kunkel. 2003. Muscular dystrophies: Genes to pathogenesis. Current Opinion in Molecular Genetics and Development 13: 231-238.

Durbeej, M. and K.P. Campbell. 2002. Muscular dystrophies involving the dystrophin-glycoprotein complex: an overview of current mouse models. Current Opinion in Genetics and Development 12: 349-361.

Hoffman, E.P. and L.M. Kunkel 1987. Dystrophin: the protein product of the Duchenne muscular dystrophy locus. Cell 51: 919-926.

Huard, J., Baohong, C., and Z. Qu-Petersen. 2003. Muscle-derived stem cells: potential for muscle regeneration. Birth Defects Research (Part C) 69:230-237.

Jasmin, B.J., Angus, L.M., Belanger, G., Chakkalakal, J.V., Gramolini, A.O., Lunde, J.A., Stocksely, M.A., and J. Thompson. 2002. Multiple regulatory events controlling the expression and localization of utrophin in skeletal muscle fibres: insights into a therapeutic strategy for Duchenne muscular dystrophy. Journal of Physiology-Paris. 96:31-42.

Kameya, S., Miyagoe, Y., Nonaka, I., Ikemoto, T., Endo, M., Hanaoka, K., Nabeshima, Y., and S. Takeda. 1999. α_1- syntrophin Gene Disruption Results in the Absence of Neuronal-type Nitric-Oxide Synthase at the Sarcolemma but Does Not Induce Muscle Degeneration. Journal of Biological Chemistry 274(4): 2193 – 2200.

Kaminski, H.J and F.H. Andrade. 2001. Nitric Oxide: biologic effects on muscle and role in muscle diseases. Neuromuscular Disorders 11: 517 – 524.

Kapsa, A., Kornberg, A.J., and E. Byrne. 2003. Novel therapies for Duchenne muscular dystrophy. The Lancet Neurology 2: 299-310.

Kolata, G. 1985. Closing in on the Muscular Dystrophy Gene. Science 230: 307-308.

Lawry, J. 1998. The Use of Flow Cytometry to Sort Cells or Particles. Proceedings of the Royal Microscopical Society 33: 27-29.

Mann, C.J., Honeyman, K., Cheng, A.J., Ly, T., Lloyd, F., Fletcher, S., Morgan, J.E., Partridge, T.A., and S.D. Wilton. 2001. Antisense-induced exon skipping and synthesis of dystrophin in the *mdx* mouse. Proceedings of the National Academy of Sciences of the United States of America 98: 42-47.

Makino K., Taki T., Ogura M., Handa S., Nakajima M., Kondo T., and H. Ohshima. 1993. Measurements and analyses of electrophoretic mobilities of RAW117 lymphosarcoma cells and their variant cells. Biophysical Chemistry 47: 261-5.

Michele, D.E. and K.P. Campbell. 2003. Dystrophin-glycoprotein complex: post-translational processing and dystroglycan function. Journal of Biological Chemistry 278: 15457-15460.

Mycielska, M.E., and M.B. Djamgoz. 2004. Cellular mechanisms of direct-current electric field effects: galvanotaxis and metastatic disease. Journal of Cell Science 117 (pt 9): 1631-1639.

Rafael, J.A., Tinsley, J.M., Potter, A.C., Deconinck, A.E., and K.E. Davies. 1998. Skeletal muscle-specific expression of a utrophin transgene rescues utrophin-dystrophin deficient mice. Nature Genetics. 19: 79-82.

Reid, M.B. 2001. Nitric oxide, reactive oxygen species, and skeletal muscle contraction. Medicine and Science in Sports and Exercise 33: 371-376.

Silvagno, F., Xia, H. and D.S. Bredt. 1996. Neuronal nitric oxide synthase-μ, an alternatively spliced isoform expressed in differentiated skeletal muscle. Journal of Biological Chemistry 217: 11204 – 11208.

Stamler, J.S. and G. Meissner. 2001. Physiology of nitric oxide in skeletal muscle. Physiological Reviews. 81: 209-237.

Tatsumi, R., Anderson, J.E., Nevoret, C.J., Halevy, O., and R.E. Allen. 1998. HGF/SF is present in normal adult skeletal muscle and is capable of activating satellite cells. Developmental Biology 194: 114-128.

Tidball, J.G., Spencer, M.J., Wehling, M., and E. Lavergne. 1999. Nitric-oxide Synthase Is a Mechanical Signal Transducer That Modulates Talin and Vinculin Expression. Journal of Biological Chemistry 274 (46): 33155 – 33160.

Wehling M., Spencer, M.J., and J.G. Tidball. 2001. A nitric oxide synthase transgene ameliorates muscular dystrophy in mdx mice. Journal of Cell Biology 155: 123-131.

Wokke, J.H.J. 2004. Genes, trials, and care: the dynamics of neuromuscular disease. The Lancet Neurology 3: 16.

Worton, R.G., Ray, P.N., Bodrug, S., Burghes, A.H.M., Hu, X., and M.W. Thompson. 1988. The problem of Duchenne muscular dystrophy. Philosophical Transactions of the Royal Society of London 319: 275-284.

Wozniak, A.C., Kong, J., Bock, E., Pilipowicz, O, and J.E. Anderson. 2005. Signaling satellite-cell activation in skeletal muscle: markers, models, stretch, and potential alternate pathways. Muscle and Nerve 31: 283-300.

Wozniak, A.C., Pilipowicz, O., Yablonka-Reuveni, Z., Greenway, S., Craven, S., Scott, E., and J.E. Anderson. 2003. C-Met expression and mechanical activation of satellite cells on cultured muscle fibers. Journal of Histochemistry and Cytochemistry 51: 1437-45.

7. Appendices

7.1 Flow Cytometry Data Sheet

7.1.1 Example of Histogram produced for *mdx* mouse spleen cells incubated with 20 µl BCF

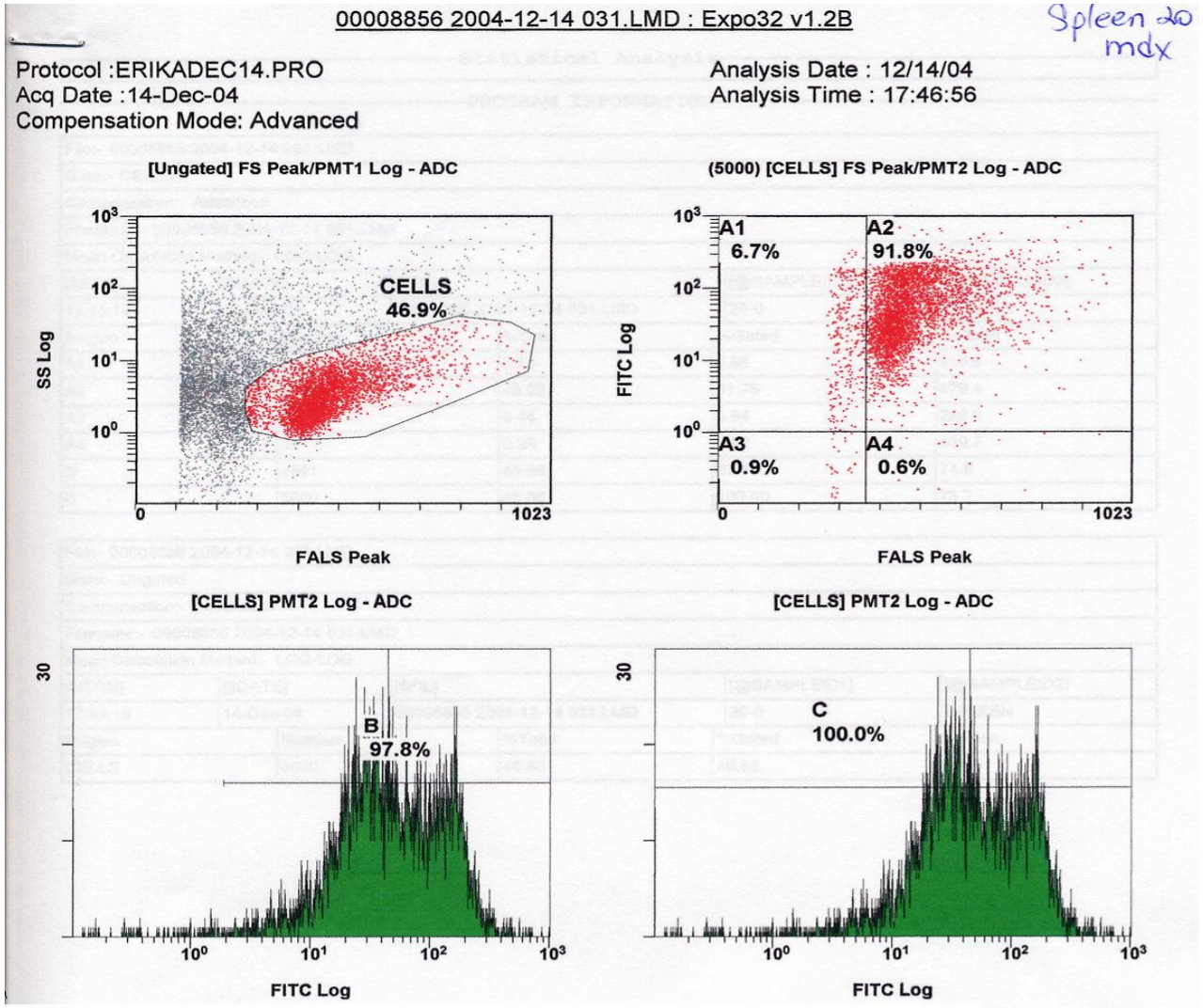

7.1.2 Statistical Printout from Flow Cytometric Analysis

* note: x-mean value used in data analysis is circled in red

Statistical Analysis

PROGRAM INFORMATION

File:- 00008856 2004-12-14 031.LMD				
Gate:- CELLS				
Compensation:- Advanced				
Filename:- 00008856 2004-12-14 031.LMD				
Mean Calculation Method:- LOG-LOG				
[$BTIM]	[$DATE]	[$FIL]	[@SAMPLEID1]	[@SAMPLEID2]
17:45:19	14-Dec-04	00008856 2004-12-14 031.LMD	20-0	SPLEEN

Region	Number	%Total	%Gated	X-Mean
A1	334	3.13	6.68	319.8
A2	4588	43.02	91.76	476.4
A3	47	0.44	0.94	296.0
A4	31	0.29	0.62	519.7
B	4891	45.86	97.82	74.8
C	5000	46.88	100.00	[illegible]

File:- 00008856 2004-12-14 031.LMD				
Gate:- Ungated				
Compensation:- Advanced				
Filename:- 00008856 2004-12-14 031.LMD				
Mean Calculation Method:- LOG-LOG				
[$BTIM]	[$DATE]	[$FIL]	[@SAMPLEID1]	[@SAMPLEID2]
17:45:19	14-Dec-04	00008856 2004-12-14 031.LMD	20-0	SPLEEN

Region	Number	%Total	%Gated	X-Mean
CELLS	5000	46.88	46.88	464.5

7.2 Recipes

7.2.1 Preparation of Proliferation Medium for C2C12 and L6 Cell Lines

1. 13.48 g of Dulbecco's Modified Eagle Medium (DMEM) powder was weighed out and dissolved in 900 ml of tissue culture grade water.

2. 1.5 g $NaHCO_3$ was added.

3. The pH of the solution was adjusted to 7.1 with continuous stirring.

4. The volume was brought up to 1000 ml.

The following steps were carried out in a laminar flow hood.

5. The medium was filter sterilized. 450 ml was put into each of two sterile bottles.

6. 1 ml antibiotic/antimycotic (Gibco©) was added per 100 ml medium.

7. 50 ml sterile fetal bovine serum and 0.05 ml 50 mg/ml Gentamycin (Gibco©) were added to each bottle.

8. Media was stored at 4°C for up to a month.

7.2.2 Preparation of Proliferation Medium for Primary Cells

1. 13.48 g of DMEM powder was weighed out and dissolved in 900 ml of tissue culture grade water.

2. 3.7 g $NaHCO_3$ was added.

3. The pH of the solution was adjusted to 7.0 with continuous stirring.

The volume was brought up to 1000 ml.

The following steps were carried out in a laminar flow hood.

4. The medium was filter sterilized. 425 ml was put into each of two sterile bottles.

5. 1 ml antibiotic/antimycotic (Gibco©) was added per 100 ml medium.

6. 75 ml sterile horse serum, 10 ml chick embryo extract, and 0.5 ml 50 mg/ml Gentamycin (Gibco©) were added to each bottle.

7. Media was stored at 4°C for up to a month.

7.2.3 Preparation of Hank's Balanced Salt Solution (10X)

1. 4.0 g KCl, 0.6 g KH_2PO_4, 80.0 g NaCl, 0.9 g Na_2HPO_4-$7H_20$, and 10.0 g D-glucose were dissolved in 850 ml double-distilled water.

2. The pH was adjusted to 7.1.

3. The volume was brought up to 1000 ml with double-distilled water.

4. The solution was filter-sterilized.